https://doi.org/10.5194/egusphere-2025-5323
Preprint. Discussion started: 12 November 2025

Rapid Secondary Organic Aerosol Formation at the Air–Water Interface from Methoxyphenols in Wildfire Emissions: UVA-Driven S(IV) Photooxidation to Organosulfates

Authors: Baohua Cai,[1] Yuanlong Huang,[2] Wenqing Jiang,[3] Yanchen Li,[1] Yali Li,[1] Jinghao Zhai,[1,4] Yaling Zeng,[1,4] Jianhuai Ye,[1,4] Huizhong Shen,[1,4] Chen Wang,[1,4] Lei Zhu,[1,4] Tzung-May Fu,[1,4] Qi Zhang,[3]* Xin Yang[1,4]*

[1]Shenzhen Key Laboratory of Precision Measurement and Early Warning Technology for Urban Environmental Health Risks, School of Environmental Science and Engineering, Southern University of Science and Technology, Shenzhen 518055, China.
[2]Ningbo Institute of Digital Twin, Eastern Institute of Technology, Ningbo 315201, China.
[3]Department of Environmental Toxicology, University of California, Davis, California 95616, United States.
[4]Guangdong Provincial Field Observation and Research Station for Coastal Atmosphere and Climate of the Greater Bay Area, Southern University of Science and Technology, Shenzhen, Guangdong, 518055, China
*Qi Zhang and Xin Yang.

Email: yangx@sustech.edu.cn and dkwzhang@ucdavis.edu
Keywords: Photooxidation, Atmospheric Organosulfates, Sulfate.

This PDF file includes:

Main Text
Figures 1 to 6
Table 1

https://doi.org/10.5194/egusphere-2025-5323
Preprint. Discussion started: 12 November 2025

Abstract

Wildfire emissions release large amounts of methoxyphenols, which serve as key precursors of aqueous-phase secondary organic aerosols (SOA). Their transformation is closely coupled with aqueous S(IV) oxidation, jointly driving the formation of sulfate and organosulfates; however, the underlying mechanisms remain poorly understood. Here, we identify a novel, metal-free mechanism for $SO_4^{\bullet-}$ generation under UVA light (370 nm), supported by experiments and quantum chemical calculations. Photolysis of the $[SO_3^{2-}+O_2]$ complex yields a $[SO_3^{\bullet-}+O_2^{\bullet-}]$ pair that forms peroxomonosulfate ($SO_5^{\bullet-}$) and ultimately $SO_4^{\bullet-}$. These radicals rapidly oxidize guaiacol, a biomass burning phenol, in bulk solution ($k = 3.8 \times 10^{10}$ M^{-1} s^{-1}), producing SOA enriched in organosulfates. Microdroplet experiments show 100-fold rate enhancement due to interfacial effects. Box and global modeling indicate that this aqueous UVA pathway is a significant, previously overlooked source of sulfate. This work established a new photochemical link between S(IV) oxidation and SOA formation, with implications for aerosol composition, oxidative capacity, and climate-relevant processes.

Abstract Graphic

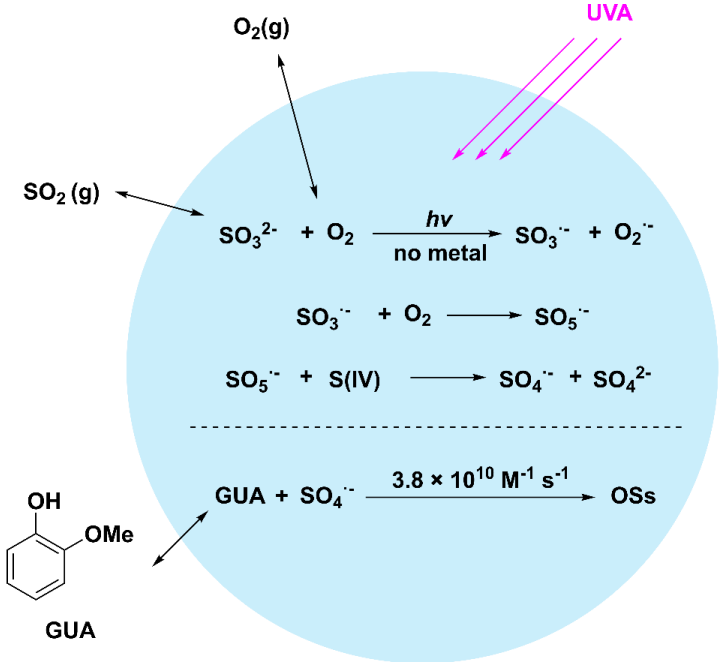

1 INTRODUCTION

https://doi.org/10.5194/egusphere-2025-5323
Preprint. Discussion started: 12 November 2025

Wildfires are occurring with increasing frequency, intensifying climate perturbation and exacerbating human health risks (Zhao et al., 2025; Teymoor Seydi et al., 2025). Their emissions, rich in methoxyphenols and other semi-volatile organic compounds, readily partition into cloud and aerosol water, where they undergo rapid transformations that produce substantial amounts of SOA (He et al., 2024; Li et al., 2023a; Liu et al., 2022). These aqueous-phase reactions are not isolated; rather, they are intricately coupled with other atmospheric chemical processes, resulting in complex multiphase chemistry that remains poorly understood.

Sulfate is a major component of fine particulate matter (PM), with significant impacts on air quality and public health (Wang et al., 2016; Abbatt et al., 2006). In the atmosphere, sulfate forms primarily through gas-phase SO_2 oxidation by hydroxyl radicals (•OH) and aqueous-phase oxidation of S(IV) species, such as dissolved SO_2, HSO_3^-, and SO_3^{2-}, in cloud, fog, or aerosol water. The aqueous-phase pathway includes direct oxidation by H_2O_2 (Liu et al., 2020), O_3 (Hoffmann, 1986; Lan et al., 2011), and NO_2 (Zhang and Chan, 2023; Gao et al., 2022; Liu and Abbatt, 2021); catalytic oxidation mediated by transition metal ions (e.g., Fe and Mn) (Zuo et al., 2005; Wang et al., 2021; Harris et al., 2013; Brandt and Eldik, 1995); and photocatalytic processes involving humic-like substances (HULIS) in the presence of O_2 (Wang et al., 2024; Pan et al., 2024). Despite extensive research, substantial discrepancies remain between observed sulfate levels and model predictions, indicating missing or poorly characterized pathways (Zheng et al., 2015).

Beyond sulfate formation, aqueous S(IV) oxidation can also form organosulfates (OSs) in the presence of volatile organic compounds (VOCs) (Passananti et al., 2016; Duporté et al., 2020; Surratt et al., 2008; Iinuma et al., 2007; Darer et al., 2011; Riva et al., 2015). OSs constitute a substantial fraction (e.g., 5-30%) of the organic mass in atmospheric PM (Shakya and Peltier, 2015; Tolocka, 2012; Hughes et al., 2021; Romero and Oehme, 2005) and provide an important chemical link between sulfur and organic aerosols. As amphiphilic molecules, OSs affect aerosol surface activity and hygroscopicity (Riva et al., 2019), thereby enhancing their potential to act as cloud condensation nuclei (CCN) (Peng et al., 2021). Some OSs are also linked to adverse health outcomes, including oxidative stress and proinflammatory responses in human lung cells (Khan et al., 2023).

The sulfate radical ($SO_4^{\bullet-}$) is a highly reactive intermediate in aqueous-phase S(IV) oxidation (Rudzinski et al., 2009), capable of rapidly oxidizing a wide variety of VOCs, including aldehydes (Coddens et al., 2018; Tran et al., 2022), olefins (Schindelka et al., 2013; Ren et al., 2021), phenols (Cope et al., 2022), and polycyclic aromatic hydrocarbons (Wang et al., 2008). These reactions produce oxidized organics that can subsequently form OSs through acid-catalyzed esterification or radical termination reactions. Solar radiation is a key driver of such radical chemistry, including the generation of $SO_4^{\bullet-}$ (George et al., 2015; Herrmann et al., 2015). For example, in high-ionic-strength aerosol solutions (e.g., 3.7 M ammonium sulfate), $SO_4^{\bullet-}$ forms under UVB (~ 310 nm) irradiation, reaching steady-state concentrations near 10^{-12} M (Cope et al., 2022). While direct photolysis of S(IV) species by UVC radiation can also yield $SO_4^{\bullet-}$ (Cao et al., 2021), UVC is largely absorbed by the stratosphere and thus negligible in the troposphere.

https://doi.org/10.5194/egusphere-2025-5323
Preprint. Discussion started: 12 November 2025

Although UVA radiation is the dominant solar band at the Earth's surface, its role in aqueous S(IV) oxidation remains poorly understood. A recent study suggests that UVA light can promote SO_2 oxidation at the air-water interface (Gong et al., 2022), but the mechanisms and broader implications are unclear. To address this gap, we combined laboratory experiments with quantum chemical calculations to investigate a novel, metal-free UVA-induced pathway for $SO_4^{\bullet-}$ generation. Using guaiacol (GUA), a representative biomass burning phenol, as a molecular probe, we tracked radical activity and OSs formation. We also explored how droplet microphysics and interfacial effects enhance this chemistry. Our findings reveal a previously overlooked UVA-driven mechanism for sulfate and OSs formation, with important implications for atmospheric chemistry, air quality, and climate.

2 MATERIALS AND METHODS

2.1 Materials

Guaiacol (99%), sodium sulfite (Na_2SO_3, >99%), 2,2,6,6-tetramethyl-1-piperinedinyloxy (TEMPO, 98%), ethanol (99%), and tert-butanol (99%) were purchased from Macklin. Zero air is made up of 21% O_2 and 79% N_2. All water used in the experiments was ultrapure Milli-Q water (18.2 MΩ·cm^{-1}).

2.2 Experimental Methods

Bulk aqueous experiment. All experiments were performed in a 25 mL airtight Pyrex tube equipped with a magnetic stir bar and a gas inlet tube for feeding high-purity zero air or nitrogen under 370 nm light or LED light irradiation. A 20 mL reaction solution containing guaiacol, Na_2SO_3, and other reactants was prepared. The pH of the reaction solution was adjusted using H_2SO_4 and NaOH and measured with a pH meter REDOX potentiometer Conductivity meter (AZ-86555) that was calibrated with commercial pH standards. In experiments requiring the measurement of total inorganic sulfur, the pH is adjusted with either phosphoric acid or phosphate. Aliquots (3 mL) were sampled every 20 min for 1h, with 0.30 mL MeOH added immediately to quench the reaction. Each experiment was repeated at least twice.

HPLC analysis. The concentrations of the guaiacol and phenol were determined using an HPLC (Thermo Scientific™ UltiMate™ 3000) equipped with a diode array detector (DAD) and an Agilent 5 TC-C18 column (150×4.60 mm, 5 μm). The column temperature was maintained at 25 ºC, and the flow rate was set to 1 ml/min. Detection was performed at 274 nm. The mobile phase consisted of 60/40 (v/v) acetonitrile/water acidified with 0.1% trifluoroacetic acid (TFA).

Direct infusion HRMS. Reaction solutions were filtered through a membrane and then directly introduced into an Agilent 6546 quadrupole time-of-flight mass spectrometer (QTOF-MS, Santa Clara, CA) with electrospray ionization (ESI) source in negative mode. The MS parameters were as follows: nebulizer, 25 psi; gas flow, 10 L/min; sheath gas temperature, 330 ºC; capillary voltage, 3500 V; sheath gas flow, 12 L/min. MS data were collected in an m/z range of 90-500. Agilent MassHunter Qualitative Analysis software (version 10.0) was used for data analysis.

https://doi.org/10.5194/egusphere-2025-5323
Preprint. Discussion started: 12 November 2025

UV-vis spectroscopy. An ultraviolet-visible Spectrophotometer (Youke, T2602, Shanghai, China) was used to monitor guaiacol absorbance during reaction with Na_2SO_3 and to record sample spectra from 200 to 500 nm. The reaction solution was directly loaded without dilution or modification. Spectra of the guaiacol – Na_2SO_3 reaction were collected every 20 min for 1 h.

IC measurements. Sulfite (SO_3^{2-}) and sulfate (SO_4^{2-}) concentrations were analyzed using a Metrohm 883 Basic IC system quipped with a Metrosep A supply 5-250/4.0 analytical column and a conductivity detector (Liu et al., 2025). Prior to analysis, 2% isopropanol and 1.0 mM NaOH was added into the reaction solution. The eluent used was 3.2 mM Na_2CO_3/1.0 mM $NaHCO_3$, with a flow rate of 0.8 mL min^{-1}. For total inorganic sulfur analysis, samples were pre-oxidized to SO_4^{2-} using hydrogen peroxide (H_2O_2) before IC detection.

FIDI-MS experiment. Droplets approximately 2 mm in diameter (~4 μL volume) were suspended from the tip of a stainless-steel capillary, which was positioned equidistantly between two parallel plate electrodes separated by 6.3 mm apart. The droplets were formed by injecting the analyte solution through the capillary using a syringe pump. The parallel plates were mounted on a translation stage to align the front electrode's aperture with the atmospheric pressure inlet of a Thermo-Fischer LTQ-XL mass spectrometer (Waltham, MA), which was operated under laboratory ambient air. Once the droplets were formed, a 60-second equilibration period was allowed to enable compound diffusion and achieve equilibrium coverage at the air-water interface.

Sampling of the suspended droplets was accomplished by applying a high-voltage pulse (3 - 5 kV, 100 ms duration, variable polarity) to the rear electrode and capillary, with half the voltage simultaneously applied to the rear plate, thereby establishing a uniform electric field. This field induced a dipole in the suspended droplets, causing it to elongate and form a double Taylor cone at both ends, which ejected oppositely charged submicron-sized droplets. These negatively charged droplets passed through the aperture of the front plate and entered the mass spectrometer for gas-phase ion detection. Due to the significant disturbance caused by the ionization droplet interface (IDI) sampling, a new droplet was generated for each measurement. In this study, a negative voltage polarity was applied to the rear plate and capillary to facilitate detection of deprotonated guaiacol ions ($[GUA]^-$).

HR-ToF-AMS experiment. During photochemical experiments, reaction solutions were aerosolized with a constant output atomizer (TSI Inc.) using N_2 as the carrier gas. The resulting aerosols were dried with a diffusion dryer and then introduced into a high-resolution time-of-flight aerosol mass spectrometer (HR-ToF-AMS; Aerodyne Research, Inc.) for chemical characterization. Drying allowed evaporation of volatile and semi-volatile species; therefore, the AMS primarily measured the mass concentration and bulk composition of the remaining low-volatility products. The operating principles of AMS have been described previously (Decarlo et al., 2006; Canagaratna et al., 2007). Briefly, the AMS analyzes non-refractory aerosols that vaporize at ~600 °C under high vacuum via 70 eV electron impact ionization. In this study, the AMS was operated in "V" ion optical mode (mass resolution ~3000) to acquire mass spectra up to m/z 422. The AMS

https://doi.org/10.5194/egusphere-2025-5323
Preprint. Discussion started: 12 November 2025

data were processed with the standard AMS toolkits SQUIRREL (v1.67) and PIKA (v1.27), available at http://cires.colorado.edu/jimenez-group/ToFAMSResources/ToFSoftware/.

2.3 Theoretical Calculations

DFT and TDDFT calculations. Geometry optimizations and frequency calculation for all molecular structures (reactants, products, and transition states) were performed using the M06-2X (Zhao and Truhlar, 2007) functional with the ma-TZVP basis set (Zheng et al., 2010), employing the SMD solvation model (Marenich et al., 2009) to simulate aqueous-phase effects in water, as implemented in the Gaussian 16 software package (Frisch et al., 2016). Optimized structures were verified by frequency computations to confirm local minima (zero imaginary frequencies) or transition structures (single imaginary frequency). Intrinsic reaction coordinate (IRC) calculations were performed to ensure that the first-order saddle points found were true transition states (TS) connecting the reactants and the products. Single-point energy calculations and solvation effects were evaluated at the CCSD(T)/aug-cc-pVTZ (Guo et al., 2018; Noga and Bartlett, 1987) level using the SMD solvation model, with geometries optimized at M06-2X/ma-TZVP and zero-point energy (ZPE) correction applied. The calculations were carried out using the ORCA 5.0.3 program package (Neese, 2012). Multiwfn 3.8 (Lu and Chen, 2012) and Shermo 2.4 (Lu and Chen, 2021) were used for further data analysis.

Classical MD calculations. Classical molecular dynamics (MD) calculations were performed using GROMACS 4.5.5 (Hess et al., 2008). In a cubic box with periodic boundary conditions, the system consisted of 1000 SPC/E water molecules and one GUA molecule using the OPLS-AA force field. Electrostatics were treated with the particle-mesh Ewald (PME) method; van der Waals interactions were truncated at 10 Å. A leap-frog integrator was used with a 2 fs timestep, and the trajectories were recorded every 10 steps.

Umbrella Sampling: To determine the average volume for each system, 10 ns simulations were conducted in the NVT ensemble, where the temperature was set to 300 K using the V-rescale method. The potentials of mean force (PMF) were calculated using the Weighted Histogram Analysis Method (WHAM) calculations, which were performed in one additional 10 ns simulation with initial configurations from the preceding simulations. The GUA moved in the z-dimension around their frozen positions under a harmonic restoring force. The force constant was set at 1×10^3 (kJ/mol/nm), and configurations were recorded every 0.5 ps. Visualization and trajectory analysis were implemented using VMD (Humphrey et al., 1996).

2.4 Model Calculation

Box model conditions. Under illumination from the Kessil PR160L-370nm lamp, the observed photooxidation rate constant (k_{obs}) for S(IV) is described by the following equation for pH ≥ 4.0:

$-d[S(IV)]/dt = k\,[H^+]^{-0.47}[O_2]\,[S(IV)]$, where $k = 6.6 \times 10^{-3}$

The lamp's intensity in the 340 - 400 nm range was measured as 850 W m^{-2} using a PL-MW2000 strong light optical power meter (Beijing Perfectlight Technology Co., Ltd.), compared 63.3 W m^{-2} for solar AM0

https://doi.org/10.5194/egusphere-2025-5323
Preprint. Discussion started: 12 November 2025

radiation in the same range (John H. Seinfeld and Pandis, 2016). Therefore, the S(IV) photooxidation rate under sunlight is approximately 7.4% of that under the Kessil PR160L-370nm lamp. Sulfate production rates at 271 K were calculated for different aqueous-phase reaction pathways with O_3, H_2O_2, TMIs, and NO_2, following Cheng (Cheng et al., 2016), excluding ionic strength effects.

The Henry's law constants at 271 K for SO_2, O_3, H_2O_2, and NO_2 are 3.521 M/atm, 0.025 M/atm, 1.147×10^6 M/atm, and 2.319×10^{-2} M/atm, respectively. Equilibrium constants for $SO_2 \cdot H_2O$ are $K_{S1} = 0.025$ M and $K_{S2} = 1.09 \times 10^{-7}$ M (Cheng et al., 2016).

Scenario Conditions. "Cloud droplets" scenario: $[SO_2(g)] = 5$ ppb, $[NO_2(g)] = 1$ ppb, $[H_2O_2(g)] = 1$ ppb, $[O_3(g)] = 50$ ppb, [Fe(III)] = 0.3 μM, [Mn(II)] = 0.03 μM, liquid water content (LWC) = 0.1 g/m^3.

"Beijing haze" scenario: $[SO_2(g)] = 40$ ppb, $[NO_2(g)] = 66$ ppb, $[H_2O_2(g)] = 0.01$ ppb, $[O_3(g)] = 1$ ppb, LWC = 300 μg/m^3. The concentrations of Fe(III) and Mn(II) were assumed to vary with pH (Cheng et al., 2016).

Globel seasonal simulation. Using global SO_2 concentrations (Fig. S24), cloud pH (Fig. S25), global aqueous-phase S(IV) concentration (Fig. S26), liquid water content (Fig. S27), and UVA radiation (345 - 412.5 nm; Fig. S28), we estimated global aqueous-phase sulfate production rates.

The aqueous-phase S(IV) concentration was calculated as:

$$[S(IV)]\ (M) = [SO_2]_g\ (ppb) \times 10^{-9} \times \left(1 + \frac{K_{s1}}{[H^+]} + \frac{K_{s1} \times K_{s2}}{[H^+]^2}\right) \times H_{so2}$$

The sulfate production rate was calculated using:

$$P[SO_4^{2-}]\ (\mu g\ m^{-3}\ h^{-1}) = \frac{UVA\ (W\ m^{-2})}{850\ (W\ m^{-2})} \times k_{obs}\ (mol\ L^{-1}\ s^{-1}) \times \frac{LWC\ (kg\ m^{-3})}{\rho\ (kg\ L^{-1})} \times 96\ (g\ mol^{-1}) \times 3600\ (s\ h^{-1}) \times 10^6\ (\mu g\ g^{-1})$$

where UVA is in W m^{-2}, k_{obs} in mol L^{-1} s^{-1}, LWC in kg m^{-3}, and ρ is the water density (kg L^{-1}).

Global distributions of SO_2, LWC, and cloud pH were derived using the GEOS-Chem Classic v14.0.2 model (Bey et al., 2001), driven by MERRA-2 meteorological product from the Goddard Earth Observing System (GEOS) of the NASA Global Modeling and Assimilation Office (GMAO). SO_2 emissions were taken from the Community Emissions Data System (CEDS) inventory (Hoesly et al., 2018). Simulations were conducted at 4° × 5° resolution with 72 vertical layers from the surface to 0.01 hPa, and results were analyzed after a 2-year spin-up.

3 RESULTS AND DISCUSSION

3.1 Photooxidation of Na_2SO_3 solution under 370 nm irradiation. To simulate atmospheric aqueous-phase SO_2 oxidation, Na_2SO_3 solutions with controlled initial pH were prepared and continuously bubbled with zero air (Fig. S1). At pH 4.0 and 0.5 mM Na_2SO_3, sulfite loss in the dark was slow, with an observed rate constant of 2.27×10^{-5} s^{-1} (Fig. S2) (Brandt and Eldik, 1995). Under UVA irradiation (370 nm; light spectrum

https://doi.org/10.5194/egusphere-2025-5323
Preprint. Discussion started: 12 November 2025

shown in Fig. S3A), the sulfite loss rate increased nearly tenfold to 2.02×10^{-4} s^{-1}, with sulfate (SO_4^{2-}) as the primary product (Fig. S4). Increasing Na_2SO_3 concentration to 2.0 mM had only a moderate effect, with rate constants averaging $(2.41 \pm 0.79) \times 10^{-4}$ s^{-1} (Fig. S5 and S6). In contrast, pH significantly influenced photooxidation kinetics (Fig. S7): the apparent sulfite decay rate increased by nearly 14-fold from pH 4.0 to 7.0, reflecting shifts in dominant S(IV) species (HSO_3^- vs. SO_3^{2-}) with different photochemical reactivities. These findings demonstrate that UVA light substantially enhances S(IV) oxidation in metal-free systems and that the reaction is strongly pH-dependent.

3.2 Photodegradation of Guaiacol in Na_2SO_3 solution. Guaiacol (GUA), a methoxyphenol emitted primarily from biomass burning (4.7 Tg yr^{-1} globally) (Liu et al., 2022; Li et al., 2023a), was used as a molecular probe to trace reactive intermediates formed during UVA-driven S(IV) oxidation. Given its Henry's law constant (Mcfall et al., 2020), up to 40% of atmospheric GUA can partition into the aqueous phase (Fig. S8), making it a relevant proxy for aqueous-phase organic transformations.

At pH 4.0, GUA (0.1 mM) was added to 2.0 mM Na_2SO_3 solution under continuous zero-air bubbling. GUA remained stable in the dark, with minor losses attributed to evaporation (Fig. 1A). Under UVA irradiation (370 nm), however, it degraded rapidly following pseudo-first-order kinetics ($k \approx 0.023$ min^{-1}; Fig. S9A) that is approximately 14 times faster than direct photolysis (Fig. S9B), highlighting the critical role of S(IV)-derived reactive intermediates. Suppressing O_2 via N_2 purging significantly reduced GUA degradation (Fig. 1A), and no degradation was observed under visible light (> 400 nm; Fig. S3B), confirming the importance of O_2-dependent photochemistry induced by UVA (Fig. S10).

We further investigated how reagent concentrations influence degradation kinetics. At high Na_2SO_3 : GUA molar ratios (≥ 20), GUA degradation followed pseudo-first-order kinetics, with rates increasing linearly with Na_2SO_3 concentration (Fig. 1B). At lower ratios, deviations from first-order behavior were observed (Fig. S11), suggesting a shift in the limiting reagent or changes in radical propagation dynamics.

3.3 Formation of organosulfates and steady-state $SO_4^{\bullet-}$ concentration. Figure S12 presents the kinetics of UVA-irradiated solutions containing 0.1 mM GUA and 0.5 mM Na_2SO_3. The apparent oxidation rate constant for SO_3^{2-} was 6.34×10^{-4} s^{-1} (Fig. S13), about three times higher than that without GUA (2.02×10^{-4} s^{-1}) (Fig. S4B), indicating that GUA significantly promoted S(IV) oxidation. The concurrent decrease in total inorganic sulfur closely tracked GUA degradation, suggesting that GUA reacted with photochemically generated intermediates to form S-containing organic species, such as organosulfates (OSs).

High-resolution mass spectrometry (HRMS; $m/\Delta m = 5 \times 10^4$) was used to identify reaction products. Negative-mode ESI analysis of a solution containing 0.1 mM GUA and 2.0 mM Na_2SO_3 at pH 4.0 (Fig. 2A) revealed unreacted GUA ($C_7H_7O_2^-$, m/z = 123.0446) along with multiple sulfate ester derivatives: $C_6H_5O_5S^-$ (m/z = 188.9858), $C_7H_7O_5S^-$ (m/z = 203.0014), $C_7H_7O_6S^-$ (m/z = 218.9963), and $C_7H_7O_7S^-$ (m/z = 234.9912).

https://doi.org/10.5194/egusphere-2025-5323
Preprint. Discussion started: 12 November 2025

These signals indicate OSs formation from GUA reacting with $SO_4^{\bullet-}$ radicals photochemically generated from SO_3^{2-} and O_2 under UVA.

To verify $SO_4^{\bullet-}$ involvement, we introduced 2,2,6,6-tetramethyl-1-piperinedinyloxy (TEMPO; $C_9H_{18}NO$) as a radical scavenger (Bai et al., 2016). In the Na_2SO_3 + TEMPO system without UVA (Fig. 2B) or after 30 minutes in the dark (Fig. 2C), only the $TEMPO^+$ - SO_3^{2-} adduct ($C_9H_{18}NO_4S^-$, m/z = 236.0968) was observed. However, under 370 nm irradiation, new peaks appeared at m/z = 252.0903 and 220.1019, corresponding to the TEMPO-$SO_4^{\bullet-}$ adduct ($C_9H_{18}NO_5S^-$) and its O_2-loss fragment ($C_9H_{18}NO_3S^-$, Fig. 2D), respectively, confirming $SO_4^{\bullet-}$ generation.

Finally, adding TEMPO to the GUA + Na_2SO_3 + UVA system (Fig. 2E) eliminated all OS peaks, leaving only signals for the TEMPO-$SO_4^{\bullet-}$ adduct and its fragment. This demonstrates that TEMPO scavenged $SO_4^{\bullet-}$ and suppressed GUA-derived OS formation, confirming $SO_4^{\bullet-}$ as the key intermediate driving the observed OSs production.

$SO_4^{\bullet-}$ can also oxidize water or OH^- to form hydroxyl radicals (•OH) (Wojnárovits and Takács, 2019), which effectively oxidize GUA in aqueous phase (Yu et al., 2014). To assess the relative contributions of •OH versus $SO_4^{\bullet-}$, we used ethanol (EtOH) and *tert*-butyl alcohol (*t*BuOH) as radical scavengers: EtOH reacts rapidly with both •OH (1.2×10^9 M^{-1} s^{-1}) and $SO_4^{\bullet-}$ (1.6×10^7 M^{-1} s^{-1}), while *t*BuOH reacts primarily with •OH (3.8×10^8 M^{-1} s^{-1}) and only weakly with $SO_4^{\bullet-}$ (4×10^5 M^{-1} s^{-1}) (Liang and Su, 2009). At pH 4.0, adding 0.5 M EtOH significantly suppressed GUA photodegradation, while *t*BuOH had little effect, supporting $SO_4^{\bullet-}$ as the dominant oxidant (Fig. S14).

The second-order rate constant for GUA + $SO_4^{\bullet-}$ was determined using the relative rate method, with phenol (k = 8.8×10^9 M^{-1} s^{-1}) as a reference (Fig. S15A) (Tran et al., 2022; Liang and Su, 2009). After accounting for direct photodegradation, the rate constant for GUA + $SO_4^{\bullet-}$ was 3.78 (± 0.42) × 10^{10} M^{-1} s^{-1}, which agrees well with the rate constant obtained from quantum chemical calculations (Li et al., 2023b). From pseudo-first-order kinetics (Fig. 1B), the steady-state concentration of $SO_4^{\bullet-}$ under varying [Na_2SO_3] was estimated to be on the order of ~ 10^{-14} M (Fig. S15B).

3.4 Photochemical Pathway of $SO_4^{\bullet-}$ formation from Na_2SO_3 under UVA irradiation. In aqueous Na_2SO_3, the primary S(IV) species are SO_2•H_2O, HSO_3^-, and SO_3^{2-}, with HSO_3^- dominant under the experimental pH range (Fig. S16). At pH 4.0, Na_2SO_3 showed nearly no UV-vis absorption above 250 nm (Fig. 3A). Adding 0.1 mM GUA introduced a strong 274 nm peak from $\pi - \pi^*$ transitions in GUA's aromatic ring. Although initial UVA absorption was minimal, it increased markedly during irradiation, indicating the formation of new light-absorbing products.

Since 370 nm UVA light (~ 3.35eV) lacks sufficient energy to directly excite either HSO_3^- or the HSO_3^--GUA complex, the formation of $SO_4^{\bullet-}$ likely involved photoactivation of intermediate complexes such as [HSO_3^- + O_2] or [SO_3^{2-} + O_2]. Time-dependent density functional theory (TDDFT) calculations support this, showing that [SO_3^{2-} + O_2] can absorb UVA light (Fig. S17) and subsequently form reactive radicals. This is

https://doi.org/10.5194/egusphere-2025-5323
Preprint. Discussion started: 12 November 2025

consistent with previous findings that halide-O_2 complexes can be photoexcited by UVA to yield radicals like X• and HO_2• (Cao et al., 2024a; Cao et al., 2024b).

Density functional theory (DFT) calculations (Fig. 3B) reveal that electron transfer from the triplet state (T1) of [SO_3^{2-} + O_2] to form $SO_3^{\bullet-}$ and $O_2^{\bullet-}$ is endergonic (~ 13 kcal/mol) and unfavorable without light. TDDFT results indicate that UVA can excite T1 to higher-energy triplet states (T2), enabling this electron transfer. The resulting $SO_3^{\bullet-}$ is oxidized by O_2 to $SO_5^{\bullet-}$, which decomposes to $SO_4^{\bullet-}$, while $O_2^{\bullet-}$ further oxidizes S(IV) species.

3.5 Mechanism of Guaiacol Photodegradation in Na_2SO_3 Solutions Under UVA Irradiation

The photodegradation of GUA in aqueous Na_2SO_3 solution under UVA irradiation proceeds through three major mechanisms, summarized in Table 1:

1) Formation of sulfur-centered radicals: Under UVA irradiation, the [SO_3^{2-} + O_2] complex is photoexcited from the triplet state (T_1) to a higher triplet (T_2), enabling electron transfer to produce $SO_3^{\bullet-}$ and $O_2^{\bullet-}$. $SO_3^{\bullet-}$ is rapidly oxidized by molecular O_2 to form $SO_5^{\bullet-}$ at a high rate ($k = 1.5 \times 10^9$ M^{-1} s^{-1}).

2) Oxidation of sulfites to sulfate: $SO_5^{\bullet-}$ reacts with HSO_3^- or SO_3^{2-} to produce $SO_4^{\bullet-}$, $SO_3^{\bullet-}$ and SO_5^{2-}. $SO_3^{\bullet-}$ re-enters the cycle by reacting with O_2 to regenerate $SO_5^{\bullet-}$. SO_5^{2-} protonates to HSO_5^-, which continues oxidizing S(IV) species to SO_4^{2-}. $O_2^{\bullet-}$ also oxidizes S(IV), but more slowly than $SO_5^{\bullet-}$ or $SO_4^{\bullet-}$ (Table S1). Importantly, $SO_5^{\bullet-}$ reacts approximately 100 times faster with SO_3^{2-} than with HSO_3^-, leading to a significant acceleration of sulfite photooxidation at pH > 4.0 where SO_3^{2-} dominates (Fig. S7).

3) Formation of organosulfates: $SO_4^{\bullet-}$ reacts with GUA extremely rapidly ($k = 3.8 \times 10^{10}$ M^{-1} s^{-1}), much faster than with S(IV) species. This rapid reaction leads to substantial formation of low-volatility organics compounds, including OSs and GUA dimers and derivatives, with a SOA yield of ~ 80% (Fig. S18). GUA also increases the overall rate of sulfite oxidation by nearly threefold (Fig. S4B and S14), probably via additional reactive radicals generated during its reaction with $SO_4^{\bullet-}$. Proposed mechanisms for the GUA-$SO_4^{\bullet-}$ reaction are shown in Fig. S19 and S20.

3.6 Photodegradation of GUA at aqueous interfaces. In atmospheric environments, cloud and fog droplets typically range from a few to tens of micrometers in diameter. Within these microdroplets, surface-active solutes often concentrate at the air-water interface, where reactions are accelerated due to surface enrichment and reduced activation energies (Ruiz-Lopez et al., 2020). Classical molecular dynamics (MD) simulations revealed that GUA is energetically favored at the interface, with an interfacial free energy 2.8 kcal/mol lower than in bulk water (Fig. 4A and S21). $SO_4^{\bullet-}$ also shows an interfacial preference, although much smaller (0.17 kcal/mol difference) (Xie et al., 2024), suggesting that both species are enriched at the interface.

Microdroplets also facilitate gas exchange, boosting [SO_3^{2-} + O_2] complex formation and $SO_4^{\bullet-}$ production under UVA. Thus, GUA photodegradation is expected to be far greater in microdroplets than in bulk water – potentially by several orders of magnitude.

https://doi.org/10.5194/egusphere-2025-5323
Preprint. Discussion started: 12 November 2025

To test this, we used field-induced droplet ionization mass spectrometry (FIDI-MS) (Huang et al., 2018; Gong et al., 2022; Zhang et al., 2023) to monitor UVA-induced photodegradation of 0.1 mM GUA in microdroplets, with and without 3.0 mM Na_2SO_3 (see Methods). Fig. 4B shows averaged FIDI-MS signals from five droplets, fitted to pseudo-first-order kinetics (Fig. S22 and S23). GUA degraded nearly 200 times faster at the interface than in bulk (k_{bulk} = 2.6 × 10^{-5} s^{-1} vs. $k_{interface}$ = 4.8 × 10^{-3} s^{-1}). With Na_2SO_3, the rate similarly increased ~ 60-fold, indicating interfacial $SO_4^{\bullet-}$ concentrations of ~10^{-12} M, about two orders magnitude higher than in bulk.

Overall, these findings demonstrate that phenolic compounds like GUA are enriched and highly reactive at air-water interfaces, where UVA-driven $SO_4^{\bullet-}$ formation greatly accelerates photodegradation and OS production.

3.7 Atmospheric Implications

When gas-phase SO_2 dissolves into cloud and fog droplets, it hydrates to from S(IV) species such as SO_3^{2-}. In the presence of O_2 and UVA irradiation, SO_3^{2-} can be oxidized to SO_4^{2-} through radical pathways. Using experimental data (Fig. S7), we derived a rate expression for sulfite oxidation at pH > 4.0. Under oxygen-saturated conditions ($[O_2]$ = 2.5 × 10^{-4} M), the rate constant is given by:

Rate constant = 1.75 × 10^{-8} × $pH^{6.23}$ (s^{-1})

Using these equations, we simulated UVA-driven sulfate formation under the AM0 standard solar spectrum and compared it with oxidation driven by conventional atmospheric oxidants (NO_2, O_3, and TMIs) (Cheng et al., 2016) (Fig. 5, see Methods). Under "Cloud droplets" conditions (John H. Seinfeld and Pandis, 2016; Herrmann et al., 2015) (Fig. 5A), UVA-driven sulfate formation in bulk solution (UVA_{low}) is comparable in magnitude to conventional pathways, with its relative importance increasing in slightly acidic environments. Under "Beijing haze" conditions (Cheng et al., 2016), even with a 50% reduction in UVA intensity, UVA-induced sulfate formation can still dominate, particularly in the presence of small droplets (UVA_{high}) (Fig. 5B).

We further modeled the global, seasonal SO_4^{2-} formation in atmospheric aqueous phases via S(IV) photooxidation of for the year 2023 (Fig. S24-28). At surface (Fig. 6) and at 1.29 km altitude (Fig. S29), SO_4^{2-} formation rates showed clear seasonal variation, with surface-level rates peaking at 1.46 × 10^{-2} μg m^{-3} h^{-1}. Higher rates were observed in regions such as Asia and South Africa, driven by elevated SO_2 emissions from industry and power generation and strong solar radiation during warmer months. In North America and the Mediterranean, despite lower SO_2 levels, higher aqueous-phase pH promotes S(IV) accumulation and accelerates oxidation rates. Over marine regions, limited direct SO_2 emissions lead to lower S(IV) concentrations than over the land. However, at 1.29 km, the greater availability of liquid water makes these areas stable and significant zones for sulfate formation, with production rates ($P[SO_4^{2-}]$) ranging from 10^{-6} to 10^{-4} μg m^{-3} h^{-1}.

https://doi.org/10.5194/egusphere-2025-5323
Preprint. Discussion started: 12 November 2025

In summary, our results reveal a previously unrecognized, metal-free pathway for SO_2 oxidation to sulfate in atmospheric aqueous phases under UVA irradiation. Unlike traditional mechanisms that rely on metal catalysts or high-energy UVB/UVC lights, we show that the $[SO_3^{2-} + O_2]$ complex can initiate sulfate radical production under UVA – wavelengths far more prevalent in the solar spectrum.

In the presence of guaiacol – a common phenolic compound from biomass burning, these sulfate radicals drive rapid GUA oxidation, producing low-volatility organic compounds, including organosulfates, at a high second-order rate constant of 3.8×10^{10} M^{-1} s^{-1}.

Moreover, microdroplet experiments show that GUA photodegradation is dramatically accelerated in small droplets under UVA light due to intensified interfacial chemistry. The high surface-area-to-volume ratio of microdroplets promotes efficient generation of reactive oxidants, particularly sulfate radicals, which accelerate both S(IV) oxidation and organics transformations. Together, these findings uncover a novel, sunlight-accessible, metal-free pathway for sulfate and SOA formation, especially relevant to slightly acidic, sunlit, and water-rich atmospheric environments.

Supplement. The supplement related to this article is available online.

Data availability. The data that support the findings of this study are available in the supplement of this article.

Author contributions. B.C., X.Y., and Q.Z. designed research; B.C., Y.H., W.J., X.Y., and Q.Z. performed research; B.C., Y.H., W.J., Y.L., Y.L., J.Z., Y.Z., J.Y., H.S., C.W., L.Z., T.F., Q.Z., and X.Y. analyzed data; B.C., Y.H., Q.Z., and X.Y. wrote the paper.

Competing interests. The contact author has declared that none of the authors has any competing interests.

Acknowledgments. Supported by Center for Computational Science and Engineering at Southern University of Science and Technology. Qi Zhang acknowledges support from the Donald G. Crosby Endowed Chair at the University of California at Davis.

Financial support. This work was supported by Shenzhen Key Laboratory of Precision Measurement and Early Warning Technology for Urban Environmental Health Risks (ZDSYS20220606100604008), Guangdong Provincial Observation and Research Station for Coastal Atmosphere and Climate of the Greater Bay Area (2021B1212050024), Shenzhen Science and Technology Program (KQTD20210811090048025, KCXFZ20230731093601003).

https://doi.org/10.5194/egusphere-2025-5323
Preprint. Discussion started: 12 November 2025

References:

Abbatt, J. P. D., Benz, S., Cziczo, D. J., Kanji, Z., Lohmann, U., and Möhler, O.: Solid Ammonium Sulfate Aerosols as Ice Nuclei: A Pathway for Cirrus Cloud Formation, Science, 313, 1770–1773, doi:10.1126/science.1129726, 2006.

Bai, C.-B., Wang, N.-X., Lan, X.-W., Wang, Y.-J., Xing, Y., Wen, J.-L., Gao, X.-W., and Zhang, W.: An Unexpected Controlled New Oxidant: $SO_4^{\cdot-}$, Sci. Rep., 6, 20163, 10.1038/srep20163, 2016.

Bey, I., Jacob, D. J., Yantosca, R. M., Logan, J. A., Field, B. D., Fiore, A. M., Li, Q., Liu, H. Y., Mickley, L. J., and Schultz, M. G.: Global modeling of tropospheric chemistry with assimilated meteorology: Model description and evaluation, J. Geophys. Res. Atmos., 106, 23073–23095, 10.1029/2001jd000807, 2001.

Brandt, C. and Eldik, R. v.: Transition Metal-Catalyzed Oxidation of Sulfur(IV) Oxides. Atmospheric-Relevant Processes and Mechanisms, Chem Rev, 95, 119–190, 10.1021/cr00033a006,, 1995.

Canagaratna, M. R., Jayne, J. T., Jimenez, J. L., Allan, J. D., Alfarra, M. R., Zhang, Q., Onasch, T. B., Drewnick, F., Coe, H., Middlebrook, A., Delia, A., Williams, L. R., Trimborn, A. M., Northway, M. J., DeCarlo, P. F., Kolb, C. E., Davidovits, P., and Worsnop, D. R.: Chemical and microphysical characterization of ambient aerosols with the aerodyne aerosol mass spectrometer, Mass Spectrom. Rev., 26, 185–222, 10.1002/mas.20115, 2007.

Cao, Y., Qiu, W., Li, J., Jiang, J., and Pang, S.: Review on UV/sulfite process for water and wastewater treatments in the presence or absence of O_2, Sci. Total Environ., 765, 142762, 10.1016/j.scitotenv.2020.142762, 2021.

Cao, Y., Liu, J., Ma, Q., Zhang, C., Zhang, P., Chen, T., Wang, Y., Chu, B., Zhang, X., Francisco, J. S., and He, H.: Photoactivation of Chlorine and Its Catalytic Role in the Formation of Sulfate Aerosols, J. Am. Chem. Soc., 146, 1467–1475, 10.1021/jacs.3c10840, 2024a.

Cao, Y., Wang, Z., Liu, J., Ma, Q., Li, S., Liu, J., Li, H., Zhang, P., Chen, T., Wang, Y., Chu, B., Zhang, X., Saiz-Lopez, A., Francisco, J. S., and He, H.: Spontaneous molecular bromine production in sea salt aerosols, Angew. Chem. Int. Ed., 63, e202409779, 10.1002/anie.202409779, 2024b.

Cheng, Y., Zheng, G., Wei, C., Mu, Q., Zheng, B., Wang, Z., Gao, M., Zhang, Q., He, K., Carmichael, G., Pöschl, U., and Su, H.: Reactive nitrogen chemistry in aerosol water as a source of sulfate during haze events in China, Sci. Adv., 2, e1601530, 10.1126/sciadv.1601530, 2016.

Coddens, E. M., Huang, L., Wong, C., and Grassian, V. H.: Influence of Glyoxal on the Catalytic Oxidation of S(IV) in Acidic Aqueous Media, ACS Earth Space Chem., 3, 142–149, 10.1021/acsearthspacechem.8b00168, 2018.

Cope, J. D., Bates, K. H., Tran, L. N., Abellar, K. A., and Nguyen, T. B.: Sulfur radical formation from the tropospheric irradiation of aqueous sulfate aerosols, Proc. Natl. Acad. Sci. U.S.A., 119, e2202857119, 10.1073/pnas.2202857119, 2022.

Darer, A. I., Cole-Filipiak, N. C., O'Connor, A. E., and Elrod, M. J.: Formation and stability of atmospherically relevant isoprene-derived organosulfates and organonitrates, Environ. Sci. Technol., 45, 1895–1902, 10.1021/es103797z, 2011.

DeCarlo, P. F., Kimmel, J. R., Trimborn, A., Northway, M. J., Jayne, J. T., Aiken, A. C., Gonin, M., Fuhrer, K., Horvath, T., Docherty, K. S., Worsnop, D. R., and Jimenez, J. L.: Field-Deployable, High-Resolution, Time-of-Flight Aerosol Mass Spectrometer, Anal. Chem., 78, 8281–8289, 10.1029/2001jd001213, 2006.

Duporté, G., Flaud, P. M., Kammer, J., Geneste, E., Augagneur, S., Pangui, E., Lamkaddam, H., Gratien, A., Doussin, J. F., Budzinski, H., Villenave, E., and Perraudin, E.: Experimental Study of

https://doi.org/10.5194/egusphere-2025-5323
Preprint. Discussion started: 12 November 2025

the Formation of Organosulfates from α-Pinene Oxidation. 2. Time Evolution and Effect of Particle Acidity, J. Phys. Chem. A, 124, 409–421, 10.1021/acs.jpca.9b07156, 2020.

Frisch, M., Trucks, G., Schlegel, H., Scuseria, G., Robb, M., Cheeseman, J., Scalmani, G., Barone, V., Petersson, G., and Nakatsuji, H.: Gaussian 16, Revision A. 03, Gaussian [code], 2016.

Gao, Y., Zhang, M., Guo, J., and Xu, L.: Impact of the oxidation of SO2 by NO2 on regional sulfate concentrations over the North China Plain, Atmos. Pollut. Res., 13, 101337, 10.1016/j.apr.2022.101337, 2022.

George, C., Ammann, M., D'Anna, B., Donaldson, D. J., and Nizkorodov, S. A.: Heterogeneous photochemistry in the atmosphere, Chem Rev, 115, 4218–4258, 10.1021/cr500648z, 2015.

Gong, C., Yuan, X., Xing, D., Zhang, D., Martins-Costa, M. T. C., Anglada, J. M., Ruiz-Lopez, M. F., Francisco, J. S., and Zhang, X.: Fast Sulfate Formation Initiated by the Spin-Forbidden Excitation of SO_2 at the Air-Water Interface, J. Am. Chem. Soc., 144, 22302–22308, 10.1021/jacs.2c10830, 2022.

Guo, Y., Riplinger, C., Becker, U., Liakos, D. G., Minenkov, Y., Cavallo, L., and Neese, F.: Communication: An improved linear scaling perturbative triples correction for the domain based local pair-natural orbital based singles and doubles coupled cluster method [DLPNO-CCSD(T)], J. Chem. Phys., 148, 011101, 10.1063/1.5011798, 2018.

Harris, E., Sinha, B., Pinxteren, D. v., Tilgner, A., Fomba, K. W., Schneider, J., Roth, A., Gnauk, T., Fahlbusch, B., Mertes, S., Lee, T., Collett, J., Foley, S., Borrmann, S., Hoppe, P., and Herrmann, H.: Enhanced Role of Transition Metal Ion Catalysis During In-Cloud Oxidation of SO_2, Science, 340, 727–730, 10.1126/science.1230911, 2013.

He, Y., Zhao, B., Wang, S., Valorso, R., Chang, X., Yin, D., Feng, B., Camredon, M., Aumont, B., Dearden, A., Jathar, S. H., Shrivastava, M., Jiang, Z., Cappa, C. D., Yee, L. D., Seinfeld, J. H., Hao, J., and Donahue, N. M.: Formation of secondary organic aerosol from wildfire emissions enhanced by long-time ageing, Nature Geoscience, 17, 124–129, 10.1038/s41561-023-01355-4, 2024.

Herrmann, H., Schaefer, T., Tilgner, A., Styler, S. A., Weller, C., Teich, M., and Otto, T.: Tropospheric aqueous-phase chemistry: kinetics, mechanisms, and its coupling to a changing gas phase, Chem Rev, 115, 4259–4334, 10.1021/cr500447k, 2015.

Hess, B., Kutzner, C., van der Spoel, D., and Lindahl, E.: GROMACS 4: Algorithms for Highly Efficient, Load-Balanced, and Scalable Molecular Simulation, J. Chem. Theory Comput., 4, 435–447, 10.1021/ct700301q, 2008.

Hoesly, R. M., Smith, S. J., Feng, L., Klimont, Z., Janssens-Maenhout, G., Pitkanen, T., Seibert, J. J., Vu, L., Andres, R. J., Bolt, R. M., Bond, T. C., Dawidowski, L., Kholod, N., Kurokawa, J.-i., Li, M., Liu, L., Lu, Z., Moura, M. C. P., O'Rourke, P. R., and Zhang, Q.: Historical (1750–2014) anthropogenic emissions of reactive gases and aerosols from the Community Emissions Data System (CEDS), Geoscientific Model Development, 11, 369–408, 10.5194/gmd-11-369-2018, 2018.

Hoffmann, M. R.: On the kinetics and mechanism of oxidation of aquated sulfur dioxide by ozone, Atmos. Environ., 20, 1145–1154, 10.1016/0004-6981(86)90147-2, 1986.

Huang, Y., Barraza, K. M., Kenseth, C. M., Zhao, R., Wang, C., Beauchamp, J. L., and Seinfeld, J. H.: Probing the OH Oxidation of Pinonic Acid at the Air–Water Interface Using Field-Induced Droplet Ionization Mass Spectrometry (FIDI-MS), J. Phys. Chem. A, 122, 6445–6456, 10.1021/acs.jpca.8b05353, 2018.

Hughes, D. D., Christiansen, M. B., Milani, A., Vermeuel, M. P., Novak, G. A., Alwe, H. D., Dickens, A. F., Pierce, R. B., Millet, D. B., Bertram, T. H., Stanier, C. O., and Stone, E. A.: $PM_{2.5}$ chemistry,

https://doi.org/10.5194/egusphere-2025-5323
Preprint. Discussion started: 12 November 2025

organosulfates, and secondary organic aerosol during the 2017 Lake Michigan Ozone Study, Atmos. Environ., 244, 117939, 10.1016/j.atmosenv.2020.117939, 2021.
Humphrey, W., Dalke, A., and Schulten, K.: VMD: Visual molecular dynamics, J. Mol. Graph., 14, 33–38, 10.1016/0263-7855(96)00018-5, 1996.
Iinuma, Y., Müller, C., Berndt, T., Böge, O., Claeys, M., and Herrmann, H.: Evidence for the Existence of Organosulfates from β-Pinene Ozonolysis in Ambient Secondary Organic Aerosol, Environ. Sci. Technol., 41, 6678–6683, 10.1021/es070938t, 2007.
John H. Seinfeld and Pandis, S. N.: ATMOSPHERIC CHEMISTRY AND PHYSICS From Air Pollution to Climate Change Third Edition, Wiley2016.
Khan, F., Chen, Y., Hartwell, H. J., Yan, J., Lin, Y.-H., Freedman, A., Zhang, Z., Zhang, Y., Lambe, A. T., Turpin, B. J., Gold, A., Ault, A. P., Szmigielski, R., Fry, R. C., and Surratt, J. D.: Heterogeneous Oxidation Products of Fine Particulate Isoprene Epoxydiol-Derived Methyltetrol Sulfates Increase Oxidative Stress and Inflammatory Gene Responses in Human Lung Cells, Chem. Res. Toxicol., 36, 1814–1825, 10.1021/acs.chemrestox.3c00278, 2023.
Lan, Y., Wheeler, S. E., and Houk, K. N.: Extraordinary Difference in Reactivity of Ozone (OOO) and Sulfur Dioxide (OSO): A Theoretical Study, J. Chem. Theory Comput., 7, 2104–2111, 10.1021/ct200293w, 2011.
Li, F., Zhou, S., Du, L., Zhao, J., Hang, J., and Wang, X.: Aqueous-phase chemistry of atmospheric phenolic compounds: A critical review of laboratory studies, Sci. Total Environ., 856, 158895, 10.1016/j.scitotenv.2022.158895, 2023a.
Li, M., Duan, P., Huo, Y., Jiang, J., Zhou, Y., Ma, Y., Jin, Z., Mei, Q., Xie, J., and He, M.: The multiple roles of phenols in the degradation of aniline contaminants by sulfate radicals: A combined study of DFT calculations and experiments, J. Hazard. Mater., 443, 130216, 10.1016/j.jhazmat.2022.130216, 2023b.
Liang, C. and Su, H.-W.: Identification of Sulfate and Hydroxyl Radicals in Thermally Activated Persulfate, Ind. Eng. Chem. Res., 48, 5558–5562, 10.1021/ie9002848, 2009.
Liu, C., Chen, D., and Chen, X.: Atmospheric Reactivity of Methoxyphenols: A Review, Environ. Sci. Technol., 56, 2897–2916, 10.1021/acs.est.1c06535, 2022.
Liu, T. and Abbatt, J. P. D.: Oxidation of sulfur dioxide by nitrogen dioxide accelerated at the interface of deliquesced aerosol particles, Nat. Chem., 13, 1173–1177, 10.1038/s41557-021-00777-0, 2021.
Liu, T., Clegg, S. L., and Abbatt, J. P. D.: Fast oxidation of sulfur dioxide by hydrogen peroxide in deliquesced aerosol particles, Proc. Natl. Acad. Sci. U.S.A., 117, 1354–1359, 10.1073/pnas.1916401117, 2020.
Liu, Y., Li, X., Ge, Q., Fang, X., Wang, T., You, W., Wang, W., Xie, L., Li, K., Gong, K., Yang, L., Wang, R., Wang, J., Wang, L., Ma, M., Huang, T., Fu, H., Chen, J., Dong, X., and Zhang, L.: Carbonate radical ion as a key driver of rapid atmospheric sulfate formation, npj Clim. Atmos. Sci., 8, 45, 10.1038/s41612-025-00905-4, 2025.
Lu, T. and Chen, F.: Multiwfn: A multifunctional wavefunction analyzer, J. Comput. Chem., 33, 580–592, 10.1002/jcc.22885, 2012.
Lu, T. and Chen, Q.: Shermo: A general code for calculating molecular thermochemistry properties, Comput. Theor. Chem., 1200, 113249, 2021.
Marenich, A. V., Cramer, C. J., and Truhlar, D. G.: Performance of SM6, SM8, and SMD on the SAMPL1 Test Set for the Prediction of Small-Molecule Solvation Free Energies, J. Phys. Chem. B, 113, 4538–4543, 10.1021/jp809094y, 2009.

https://doi.org/10.5194/egusphere-2025-5323
Preprint. Discussion started: 12 November 2025

532 McFall, A. S., Johnson, A. W., and Anastasio, C.: Air–Water Partitioning of Biomass-Burning
533 Phenols and the Effects of Temperature and Salinity, Environ. Sci. Technol., 54, 3823–3830,
534 10.1021/acs.est.9b06443, 2020.
535 Neese, F.: The ORCA program system, WIREs Comput. Mol. Sci., 73–78, 2012.
536 Noga, J. and Bartlett, R. J.: The full CCSDT model for molecular electronic structure, J. Chem.
537 Phys., 86, 7041–7050, 10.1063/1.452353, 1987.
538 Pan, Y., Zhang, F., Tan, W., and Feng, X.: New insight into wastewater treatment by activation of
539 sulfite with humic acid under visible light irradiation, Water Res., 258, 121773,
540 10.1016/j.watres.2024.121773, 2024.
541 Passananti, M., Kong, L., Shang, J., Dupart, Y., Perrier, S., Chen, J., Donaldson, D. J., and George,
542 C.: Organosulfate Formationthrough the Heterogeneous Reactionof Sulfur Dioxide with
543 Unsaturated Fatty Acids and Long-Chain Alkenes, Angew. Chem. Int. Ed., 55, 10336 –10339,
544 10.1002/anie.201605266, 2016.
545 Peng, C., Razafindrambinina, P. N., Malek, K. A., Chen, L., Wang, W., Huang, R.-J., Zhang, Y., Ding,
546 X., Ge, M., Wang, X., Asa-Awuku, A. A., and Tang, M.: Interactions of organosulfates with water
547 vapor under sub- and supersaturated conditions, Atmos. Chem. Phys., 21, 7135–7148,
548 10.5194/acp-21-7135-2021, 2021.
549 Ren, H., Sedlak, J. A., and Elrod, M. J.: General Mechanism for Sulfate Radical Addition to Olefinic
550 Volatile Organic Compounds in Secondary Organic Aerosol, Environ. Sci. Technol., 55, 1456–
551 1465, 10.1021/acs.est.0c05256, 2021.
552 Riva, M., Tomaz, S., Cui, T., Lin, Y. H., Perraudin, E., Gold, A., Stone, E. A., Villenave, E., and
553 Surratt, J. D.: Evidence for an unrecognized secondary anthropogenic source of organosulfates
554 and sulfonates: gas-phase oxidation of polycyclic aromatic hydrocarbons in the presence of
555 sulfate aerosol, Environ. Sci. Technol., 49, 6654–6664, 10.1021/acs.est.5b00836, 2015.
556 Riva, M., Chen, Y., Zhang, Y., Lei, Z., Olson, N. E., Boyer, H. C., Narayan, S., Yee, L. D., Green, H. S.,
557 Cui, T., Zhang, Z., Baumann, K., Fort, M., Edgerton, E., Budisulistiorini, S. H., Rose, C. A., Ribeiro,
558 I. O., RL, E. O., Dos Santos, E. O., Machado, C. M. D., Szopa, S., Zhao, Y., Alves, E. G., de Sa, S. S.,
559 Hu, W., Knipping, E. M., Shaw, S. L., Duvoisin Junior, S., de Souza, R. A. F., Palm, B. B., Jimenez, J.
560 L., Glasius, M., Goldstein, A. H., Pye, H. O. T., Gold, A., Turpin, B. J., Vizuete, W., Martin, S. T.,
561 Thornton, J. A., Dutcher, C. S., Ault, A. P., and Surratt, J. D.: Increasing Isoprene Epoxydiol-to-
562 Inorganic Sulfate Aerosol Ratio Results in Extensive Conversion of Inorganic Sulfate to
563 Organosulfur Forms: Implications for Aerosol Physicochemical Properties, Environ. Sci. Technol.,
564 53, 8682–8694, 10.1021/acs.est.9b01019, 2019.
565 Romero, F. and Oehme, M.: Organosulfates – A New Component of Humic-Like Substances in
566 Atmospheric Aerosols?, J. Atmos. Chem., 52, 283–294, 10.1007/s10874-005-0594-y, 2005.
567 Rudzinski, K. J., Gmachowski, L., and Kuznietsova, I.: Reactions of isoprene and sulphoxy radical-
568 anions – a possible source of atmospheric organosulphites and organosulphates, Atmos. Chem.
569 Phys., 9, 2129–2140, 10.5194/acp-9-2129-2009, 2009.
570 Ruiz-Lopez, M. F., Francisco, J. S., Martins-Costa, M. T. C., and Anglada, J. M.: Molecular
571 reactions at aqueous interfaces, Nat. Rev. Chem., 4, 459–475, 10.1038/s41570-020-0203-2,
572 2020.
573 Schindelka, J., Iinuma, Y., Hoffmann, D., and Herrmann, H.: Sulfate radical-initiated formation of
574 isoprene-derived organosulfates in atmospheric aerosols, Faraday Discuss., 165, 237–259,
575 10.1039/c3fd00042g, 2013.

https://doi.org/10.5194/egusphere-2025-5323
Preprint. Discussion started: 12 November 2025

Shakya, K. M. and Peltier, R. E.: Non-sulfate sulfur in fine aerosols across the United States: Insight for organosulfate prevalence, Atmos. Environ., 100, 159–166, 10.1016/j.atmosenv.2014.10.058, 2015.

Surratt, J. D., Gómez-González, Y., Chan, A. W. H., Vermeylen, R., Shahgholi, M., Kleindienst, T. E., Edney, E. O., Offenberg, J. H., Lewandowski, M., Jaoui, M., Maenhaut, W., Claeys, M., Flagan, R. C., and Seinfeld, J. H.: Organosulfate Formation in Biogenic Secondary Organic Aerosol, J. Phys. Chem. A, 112, 8345–8378, 10.1021/jp802310p, 2008.

Teymoor Seydi, S., Abatzoglou, J. T., Jones, M. W., Kolden, C. A., Filippelli, G., Hurteau, M. D., AghaKouchak, A., Luce, C. H., Miao, C., and Sadegh, M.: Increasing global human exposure to wildland fires despite declining burned area, Science, 389, 826–829, 10.1126/science.adu6408, 2025.

Tolocka, M. P.: Contribution of Organosulfur Compounds to Organic Aerosol Mass, Environ. Sci. Technol., 46, 7978−7983, 10.1021/es300651v, 2012.

Tran, L. N., Abellar, K. A., Cope, J. D., and Nguyen, T. B.: Second-Order Kinetic Rate Coefficients for the Aqueous-Phase Sulfate Radical ($SO_4^{\bullet-}$) Oxidation of Some Atmospherically Relevant Organic Compounds, J. Phys. Chem. A, 126, 6517–6525, 10.1021/acs.jpca.2c04964, 2022.

Wang, D., Li, Y., Yang, M., and Han, M.: Decomposition of polycyclic aromatic hydrocarbons in atmospheric aqueous droplets through sulfate anion radicals: An experimental and theoretical study, Sci. Total Environ., 393, 64–71, 10.1016/j.scitotenv.2007.11.036, 2008.

Wang, G., Zhang, R., Gomez, M. E., Yang, L., Levy Zamora, M., Hu, M., Lin, Y., Peng, J., Guo, S., Meng, J., Li, J., Cheng, C., Hu, T., Ren, Y., Wang, Y., Gao, J., Cao, J., An, Z., Zhou, W., Li, G., Wang, J., Tian, P., Marrero-Ortiz, W., Secrest, J., Du, Z., Zheng, J., Shang, D., Zeng, L., Shao, M., Wang, W., Huang, Y., Wang, Y., Zhu, Y., Li, Y., Hu, J., Pan, B., Cai, L., Cheng, Y., Ji, Y., Zhang, F., Rosenfeld, D., Liss, P. S., Duce, R. A., Kolb, C. E., and Molina, M. J.: Persistent sulfate formation from London Fog to Chinese haze, Proc. Natl. Acad. Sci. U.S.A., 113, 13630–13635, 10.1073/pnas.1616540113, 2016.

Wang, W., Liu, Y., Wang, T., Ge, Q., Li, K., Liu, J., You, W., Wang, L., Xie, L., Fu, H., Chen, J., and Zhang, L.: Significantly Accelerated Photosensitized Formation of Atmospheric Sulfate at the Air–Water Interface of Microdroplets, J. Am. Chem. Soc., 146, 6580–6590, 10.1021/jacs.3c11892, 2024.

Wang, W., Liu, M., Wang, T., Song, Y., Zhou, L., Cao, J., Hu, J., Tang, G., Chen, Z., Li, Z., Xu, Z., Peng, C., Lian, C., Chen, Y., Pan, Y., Zhang, Y., Sun, Y., Li, W., Zhu, T., Tian, H., and Ge, M.: Sulfate formation is dominated by manganese-catalyzed oxidation of SO2 on aerosol surfaces during haze events, Nat. Commun., 12, 1993, 10.1038/s41467-021-22091-6, 2021.

Wojnárovits, L. and Takács, E.: Rate constants of sulfate radical anion reactions with organic molecules: A review, Chemosphere, 220, 1014–1032, 10.1016/j.chemosphere.2018.12.156, 2019.

Xie, R., Guo, K., Li, Y., Zhang, Y., Zhong, H., Leung, D. Y. C., and Huang, H.: Harnessing air-water interface to generate interfacial ROS for ultrafast environmental remediation, Nat. Commun., 15, 8860, 10.1038/s41467-024-53289-z, 2024.

Yu, L., Smith, J., Laskin, A., Anastasio, C., Laskin, J., and Zhang, Q.: Chemical characterization of SOA formed from aqueous-phase reactions of phenols with the triplet excited state of carbonyl and hydroxyl radical, Atmos. Chem. Phys., 14, 13801–13816, 10.5194/acp-14-13801-2014, 2014.

Zhang, D., Wang, J., Chen, H., Gong, C., Xing, D., Liu, Z., Gladich, I., Francisco, J. S., and Zhang, X.: Fast Hydroxyl Radical Generation at the Air-Water Interface of Aerosols Mediated by Water-

https://doi.org/10.5194/egusphere-2025-5323
Preprint. Discussion started: 12 November 2025

621 Soluble $PM_{2.5}$ under Ultraviolet A Radiation, J. Am. Chem. Soc., 145, 6462–6470,
622 10.1021/jacs.3c00300, 2023.
623 Zhang, R. and Chan, C. K.: Simultaneous formation of sulfate and nitrate via co-uptake of SO_2
624 and NO_2 by aqueous NaCl droplets: combined effect of nitrate photolysis and chlorine
625 chemistry, Atmos. Chem. Phys., 23, 6113–6126, 10.5194/acp-23-6113-2023, 2023.
626 Zhao, J., Zheng, B., Ciais, P., Chen, Y., Gasser, T., Canadell, J. G., Zhang, L., and Zhang, Q.: Global
627 warming amplifies wildfire health burden and reshapes inequality, Nature, 10.1038/s41586–
628 41025–09612–41589, 10.1038/s41586-025-09612-9, 2025.
629 Zhao, Y. and Truhlar, D. G.: The M06 suite of density functionals for main group
630 thermochemistry, thermochemical kinetics, noncovalent interactions, excited states, and
631 transition elements: two new functionals and systematic testing of four M06-class functionals
632 and 12 other functionals, Theor. Chem. Acc., 120, 215–241, 10.1007/s00214-007-0310-x, 2007.
633 Zheng, B., Zhang, Q., Zhang, Y., He, K. B., Wang, K., Zheng, G. J., Duan, F. K., Ma, Y. L., and
634 Kimoto, T.: Heterogeneous chemistry: a mechanism missing in current models to explain
635 secondary inorganic aerosol formation during the January 2013 haze episode in North China,
636 Atmos. Chem. Phys., 15, 2031–2049, 10.5194/acp-15-2031-2015, 2015.
637 Zheng, J., Xu, X., and Truhlar, D. G.: Minimally augmented Karlsruhe basis sets, Theor. Chem.
638 Acc., 128, 295–305, 10.1007/s00214-010-0846-z, 2010.
639 Zuo, Y., Zhan, J., and Wu, T.: Effects of Monochromatic UV-Visible Light and Sunlight on Fe(III)-
640 Catalyzed Oxidation of Dissolved Sulfur Dioxide, J. Atmos. Chem., 50, 195–210, 10.1007/s10874-
641 005-2813-y, 2005.

642

643

https://doi.org/10.5194/egusphere-2025-5323
Preprint. Discussion started: 12 November 2025

644 **Figures and Tables**

645 **Figure 1.**

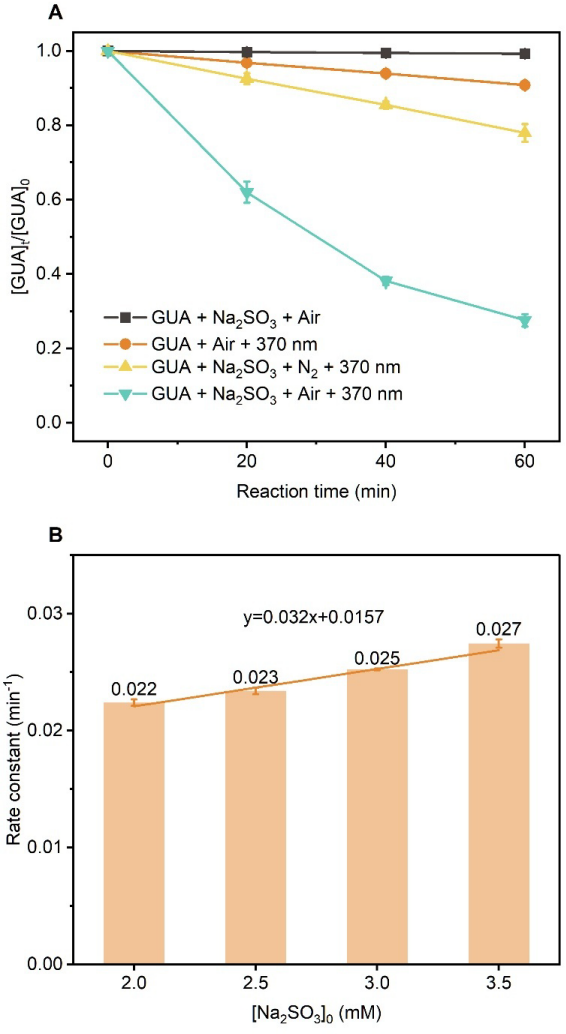

646

647 (*A*) Kinetics of the aqueous-phase reaction between guaiacol and Na_2SO_3 under different conditions. (*B*) The
648 dependence of the pseudo-first-order rate constant for GUA decay on the concentration of Na_2SO_3. Error bars
649 represent the standard deviations from independent experiments. Experimental conditions: [guaiacol] = 0.1
650 mM, [Na_2SO_3] = 2.0 mM, pH = 4.0 ± 0.1, zero-air bubbling, 370 nm light irradiation, room temperature.

651

https://doi.org/10.5194/egusphere-2025-5323
Preprint. Discussion started: 12 November 2025

652 **Figure 2.**

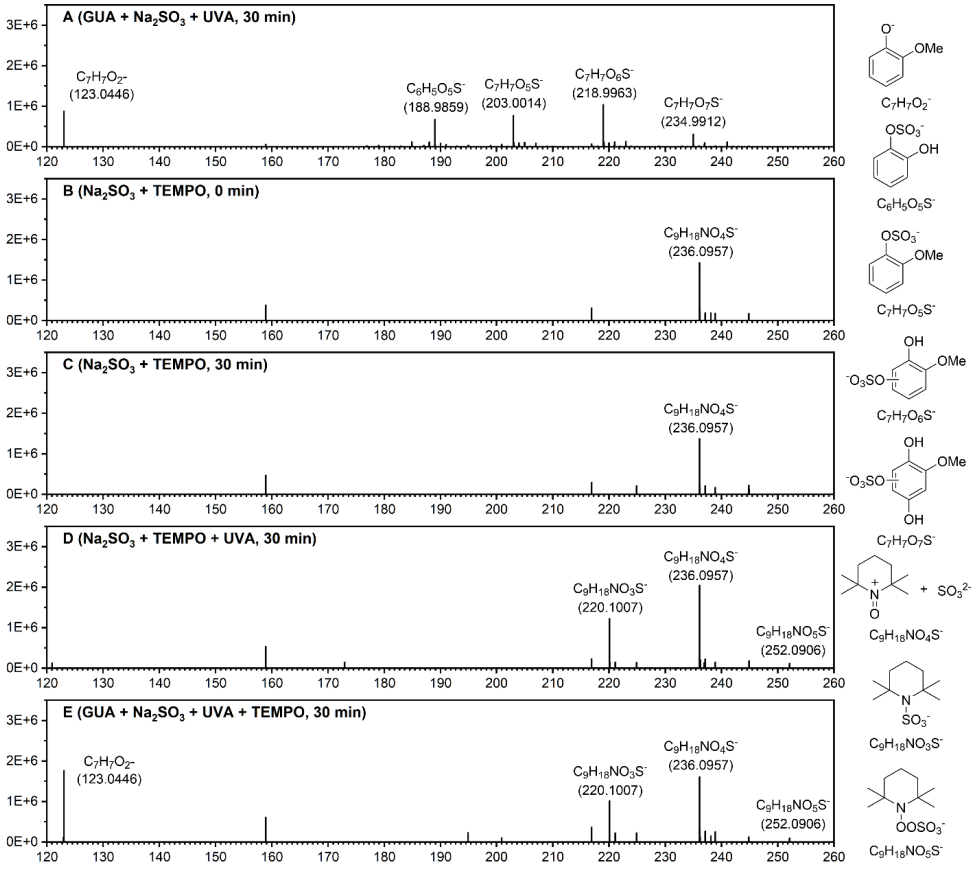

653

654 High-resolution mass spectra of reaction products from: (*A*) GUA + Na_2SO_3 under after 30 min of 370 nm
655 irradiation; (*B*) Na_2SO_3 + TEMPO at 0 min; (*C*) Na_2SO_3 + TEMPO after 30 min in the dark; (*D*) Na_2SO_3 +
656 TEMPO after 30 min of 370 nm irradiation; and (*E*) GUA + Na_2SO_3 + TEMPO after 30 min of 370 nm
657 irradiation. Experimental conditions: [guaiacol] = 0.1 mM, [Na_2SO_3] = 2.0 mM, [TEMPO] = 4.0 mM, pH =
658 4.0 ± 0.1, zero-air bubbling, and room temperature. Proposed chemical structures corresponding to the key
659 mass spectral peaks are shown to the right of the spectra.
660

https://doi.org/10.5194/egusphere-2025-5323
Preprint. Discussion started: 12 November 2025

Figure 3.

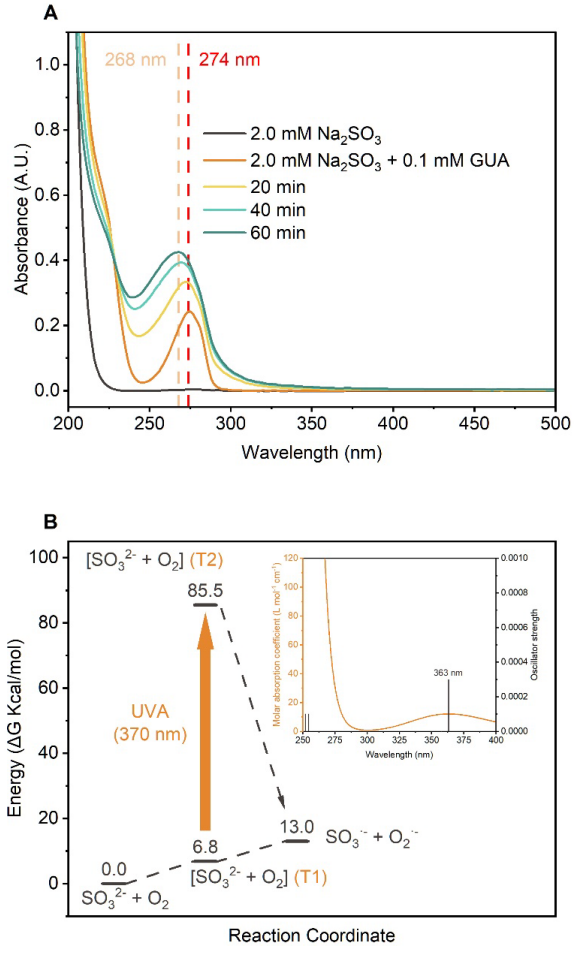

(*A*) UV-vis absorption spectra of the GUA + Na_2SO_3 reaction solution at different time points. (*B*) Gibbs free energy profiles (kcal/mol, 298.15 K) for the SO_3^{2-} + O_2 reaction, calculated at the CCSD(T)/aug-cc-pVTZ/SMD(water)//M06-2X/ma-TZVP/SMD(water) level with Zero Point Energy (ZPE) correction, with the inset showing the vertical excitation spectra of the [SO_3^{2-} + O_2] complex, calculated using TDDFT at the M06-2X/ma-TZVP/SMD(water) level.

https://doi.org/10.5194/egusphere-2025-5323
Preprint. Discussion started: 12 November 2025

669 **Figure 4.**

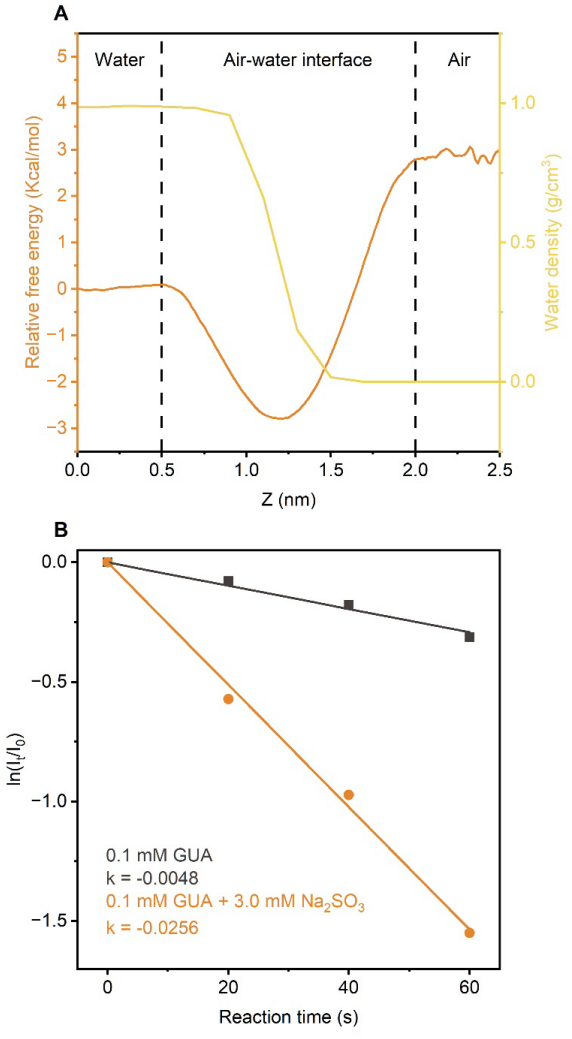

670

671 (*A*) Free energy profiles for GUA transfer from the gas phase to bulk water, overlaid with water density
672 distribution at air-water interface. (*B*) Kinetics of direct photodegradation of GUA in microdroplets, with and
673 without Na_2SO_3, under UVA irradiation.

674

https://doi.org/10.5194/egusphere-2025-5323
Preprint. Discussion started: 12 November 2025

675 **Figure 5.**

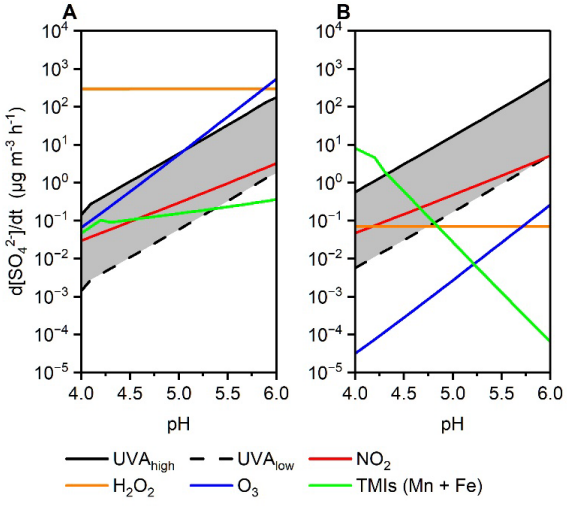

676

677 Simulated aqueous-phase sulfate production rates from SO_2 oxidation as a function of pH under two
678 atmospheric scenarios: (*A*) "Cloud droplets" scenario with full UVA intensity (AM0 standard). (*B*) "Beijing
679 haze" scenario with 50% reduced UVA intensity. Colored lines represent contributions from individual
680 oxidants and the shaded region indicates the total sulfate production range bounded by the UVA_{high} and
681 UVA_{low} estimates.
682

https://doi.org/10.5194/egusphere-2025-5323
Preprint. Discussion started: 12 November 2025

683 **Figure 6.**

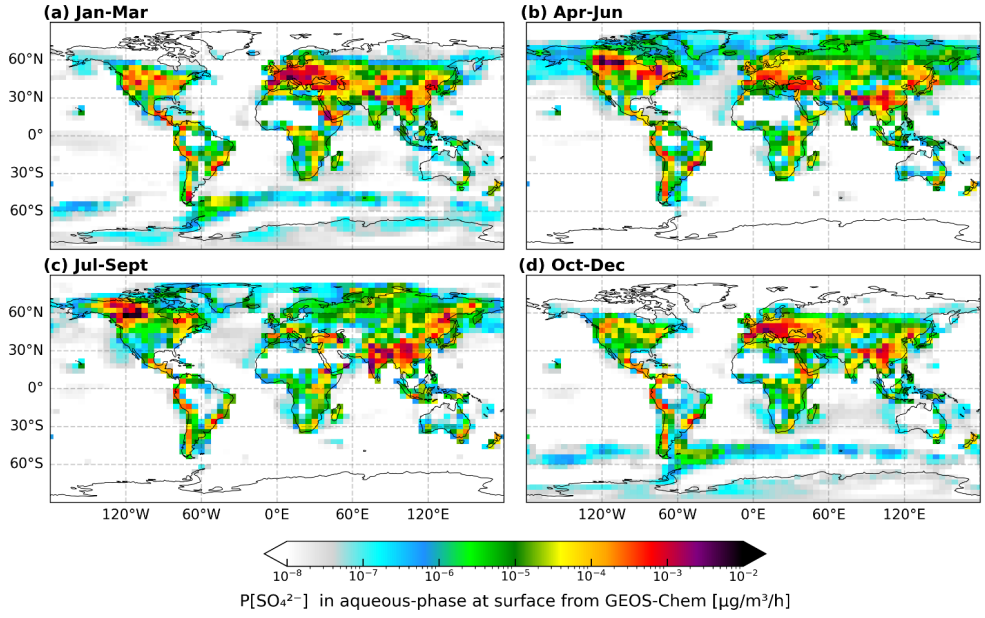

684

685 Seasonal variations in surface-level aqueous-phase SO_4^{2-} formation rates from S(IV) photoreactions in 2023.

686

https://doi.org/10.5194/egusphere-2025-5323
Preprint. Discussion started: 12 November 2025

687 **Table 1.** Reactions and rate constants of GUA photodegradation in Na_2SO_3 solutions (John H. Seinfeld and
688 Pandis, 2016; Rudzinski et al., 2009).

1) Formation of sulfur radical	
$HSO_3^- \rightarrow SO_3^{2-} + H^+$	$6.75 \times 10^3\ s^{-1}$
$SO_3^{2-} + H^+ \rightarrow HSO_3^-$	$1.0 \times 10^{11}\ M^{-1}\ s^{-1}$
$SO_3^{2-} + O_2 \rightarrow [SO_3^{2-} + O_2]$	
$[SO_3^{2-} + O_2] + UVA \rightarrow SO_3^{\bullet-} + O_2^{\bullet-}$	
$SO_3^{\bullet-} + O_2 \rightarrow SO_5^{\bullet-}$	$1.5 \times 10^9\ M^{-1}\ s^{-1}$
2) Oxidation of sulfites	
$SO_5^{\bullet-} + HSO_3^- \rightarrow SO_3^{\bullet-} + SO_5^{2-} + H^+$	$2.5 \times 10^4\ M^{-1}\ s^{-1}$
$SO_5^{\bullet-} + HSO_3^- \rightarrow SO_4^{\bullet-} + SO_4^{2-} + H^+$	$7.5 \times 10^4\ M^{-1}\ s^{-1}$
$SO_5^{\bullet-} + SO_3^{2-} \rightarrow SO_3^{\bullet-} + SO_5^{2-}$	$3.25 \times 10^6\ M^{-1}\ s^{-1}$
$SO_5^{\bullet-} + SO_3^{2-} \rightarrow SO_4^{\bullet-} + SO_4^{2-}$	$9.75 \times 10^6\ M^{-1}\ s^{-1}$
$SO_4^{\bullet-} + HSO_3^- \rightarrow SO_3^{\bullet-} + SO_4^{2-} + H^+$	$1.4 \times 10^7\ M^{-1}\ s^{-1}$
$SO_4^{\bullet-} + SO_3^{2-} \rightarrow SO_3^{\bullet-} + SO_4^{2-}$	$1.4 \times 10^7\ M^{-1}\ s^{-1}$
$SO_5^{2-} + H^+ \rightarrow HSO_5^-$	$1.0 \times 10^{10}\ M^{-1}\ s^{-1}$
$HSO_5^- \rightarrow SO_5^{2-} + H^+$	$3.98\ s^{-1}$
$HSO_5^- + HSO_3^- \rightarrow 2SO_4^{2-} + 2H^+$	$7.5 \times 10^3\ M^{-1}\ s^{-1}$
$HSO_5^- + SO_3^{2-} \rightarrow 2SO_4^{2-} + H^+$	$7.5 \times 10^3\ M^{-1}\ s^{-1}$
3) Formation of OSs	
GUA + $SO_4^{\bullet-}$ → Products (including OSs)	$3.8 \times 10^{10}\ M^{-1}\ s^{-1}$

689